The Molar Bud-to-Cap Transition is Proliferation-Independent

Shuntaro Yamada, Rupali Lav, Jingjing Li, Abigail S. Tucker and Jeremy B.A. Green*
Centre for Craniofacial Biology & Regeneration, King's College London, UK

*Correspondence: jeremy.green@kcl.ac.uk

Abstract:

Tooth germs undergo a series of dynamic morphological changes through bud, cap and bell stages, in which odontogenic epithelium continuously extends into the underlying mesenchyme. During the transition from bud to cap stage, the base of the bud flattens and then bends into a cap shape whose edges are referred to as "cervical loops". Although genetic mechanisms for cap formation have been well described, little is understood about the morphogenetic mechanisms. Computer modelling and cell trajectory tracking have suggested that the epithelial bending is driven purely by differential cell proliferation and adhesion in different parts of the tooth germ. Here we show that, unexpectedly, inhibition of cell proliferation did not prevent bud-to-cap morphogenesis. We quantified cell shapes and actin and myosin distributions in different parts of the tooth epithelium at the critical stages and found that these are consistent with basal relaxation in the forming cervical loops and basal constriction around enamel knot at the centre of the cap. Inhibition of focal adhesion kinase, which is required for basal constriction in other systems, arrested the molar explant morphogenesis at bud stage. Together these results show that the bud-to-cap transition is largely proliferation-independent and we propose that it is driven by classic actomyosin-driven cell shape-dependent mechanisms. We discuss how these results can be reconciled with the previous models and data.

Key Words: Developmental Biology, Cell biology, Morphogenesis, Morphometrics, Tooth development

Introduction

Tooth formation is a well-established model for epithelial-mesenchymal signalling interactions and for ectodermal organ formation and organogenesis in general (Pispa and Thesleff 2003; Thesleff 2003). However, until recently, the morphogenetic mechanisms of tooth development and that of other ectodermal organs were poorly understood and were generally described merely as “down growth” of the epithelium into the underlying mesenchyme (Mikkola and Millar 2006; Pispa and Thesleff 2003; Ten Cate et al. 2012), suggesting largely proliferation-driven mechanisms. Recent work has shown that tooth morphogenesis is more complex. The first step – the transition from epithelium (“lamina stage”) to an invaginated tooth bud – occurs through a combination of local (vertical-cell-division-dependent) stratification and (cell-intercalation-dependent) contraction of a canopy of suprabasal cells anchored to the basal lamina by flanking basal “shoulder” cells (Li et al. 2016; Panousopoulou and Green 2016). The contractile canopy ultimately forms the neck of the tooth bud, and this mechanism accounts for the morphogenesis from placode all the way to late bud stage (Li et al. 2016; Panousopoulou and Green 2016).

The next step of tooth germ morphogenesis is the transition from bud to cap stage. The base of the bud flattens forming epithelial bends, known as cervical loops on either side (**Fig.1**). Although known as loops because of their appearance in section, the lobes/loops are proximodistally extended ridges in molars and an annular rim in incisors (Kieffer et al. 1999; Peterkova et al. 1996).) The cervical loops become gradually deeper and curve down to make the eponymous cap shape (Fig.1) and then towards one another to make a (cow)bell shape that gives its name to the next stage. Between the cervical loops lies the inner dental epithelium (IDE), the middle of which becomes the primary enamel knot (EK). EKs are signalling centres known for having low or no cell proliferation and being the sites of future tooth cusp formation (Jernvall et al. 1994). The correlation between low proliferation in the future cusps (epithelial peaks) and higher proliferation in the valleys – the cervical loops and inter-cusp regions – has given rise to models in which differential proliferation was responsible for the epithelial morphogenesis (e.g. Salazar-Ciudad and Jernvall 2002; 2010).

During the bud-to-cap transition, the surrounding mesenchyme condenses, forming a capsule. This led to ideas that epithelial proliferation within the constraining mesenchymal capsule drives the epithelium to buckle to form the cervical loop and cusps (Morita et al. 2016; Takigawa-Imamura et al. 2015). Support for this idea came from experimental removal of the mesenchyme from late bud stage tooth explants which resulted in the cervical loops springing outwards, showing that the mesenchyme indeed constrains the epithelial shape (Morita et al. 2016). Sophisticated live explant imaging and computer modelling showed that differential proliferation and adhesion between the mesenchymal, basal and suprabasal epithelial cells, with constraint from less proliferative mesenchyme, could account for the bud-to-cap morphogenesis (Marin-Riera et al. 2018).

Although epithelial buckling due to proliferation within a constraining structure is known in other contexts (e.g. intestinal villus formation (Shyer et al. 2013)), most known epithelial bending

mechanisms rely on autonomous cell shape change, especially actin-myosin-dependent apical or basal constriction (Pearl et al. 2017). Here we show that, contrary to prevailing tooth models, inhibition of cell proliferation does not significantly inhibit bud-to-cap morphogenesis. We quantify cell shape in the tooth epithelium at bud-to-cap stages and observe basal expansion in the cervical loops and basal contraction in the juxta-knot inner dental epithelium. Actin and myosin staining suggest basal relaxation and active basal constriction for these respectively. Finally we show that inhibition of focal adhesion kinase (FAK), implicated in other instances of active basal constriction, completely inhibits bud-to-cap morphogenesis. We propose that the bud-to-cap transition is largely or entirely proliferation-independent but that prior models and data are consistent with proliferation being the driver of the subsequent cap-to-bell transition.

Materials and Methods

Animals

Animals were handled under UK Home Office Licensing and King's College London Ethics Committee approval. Pregnant wild-type CD1 mice and mT/mG (Gt(ROSA)26Sor$^{tm4(ACTB-tdTomato,-EGFP)Luo}$ (Jackson Laboratories # 007576)) mice were euthanised by cervical dislocation.

Ex vivo explant culture and drug treatment

Frontal slices containing tooth germs of E13.5, E14.0 and E14.5 mandibular molars were obtained as described (Alfaqeeh and Tucker 2013). Briefly, mandibles were manually dissected from the heads in Advanced Dulbecco's Modified Eagle Medium F12 (DMEM/F12, Gibco) and sliced frontally into 200µm sections using a McIlwain Tissue Chopper (Ted Pella, Inc., USA.). Slices were cultured on PET membranes (Corning, 353090) on a steel mesh (Goodfellow, FE228710) in DMEM/F12 with 1% Penicillin-Streptomycin (P4333, Sigma), 15% foetal calf serum and 0.1 g/l Vitamin C at 37°C in 5% CO2-humidified atmosphere. Explants were treated for with aphidicolin (2.0 µg/ml in DMSO, Santa Cruz Biotechnology). 10µM BrdU was added after 3 or 23 hours and explants fixed at 5 or 25 hours in 4% paraformaldehyde (PFA) for 4 hours at room temperature. Explants were photographed under a stereo zoom dissection microscope with brightfield optics at the 3 and 23 hour time points (to avoid the trivial shape perturbation sometimes caused by addition of the BrdU-containing medium). For FAK inhibition, explants were treated with 1 µM PF-573228 (Cayman Chemicals) in place of aphidicolin.

Tissue preparation for staining

For mT/mG cellular/nuclear morphometric analyses or actin/myosin staining, whole embryos were fixed in 4% PFA for 4h at room temperature. After a PBS wash, heads were embedded in 0.49g gelatin (Type-B bovine, Sigma-Aldrich), 30g albumin, 20g sucrose, 3.5 ml glutaraldehyde in 100ml

PBS. Gelatin blocks were re-fixed in 4% PFA at 4°C overnight and frontally sliced on a Vibratome (Leica VT1000S) at 90μm thickness.

Immunofluorescence and imaging

For BrdU staining, antigen retrieval (DNA denaturation) was performed using 10mM sodium citrate (pH6) at 95°C, 20 minutes, permeabilised in 0.1% Triton X-100 (T8787, Sigma) in PBS (PBST) for 3x10 minutes, then blocked with 20% goat serum (G6767, Sigma) in PBST for 30-60 minutes room temperature. For P-cadherin staining only, 20% donkey serum (D9663, Sigma) was used instead of goat. Specimens were incubated with primary antibodies at 4°C overnight. Primary antibodies were: anti-RFP (1:500, #600-401-379, Rockland Immunochemical), goat anti-P-cadherin (1:200, AF761, R&D Systems), rabbit anti-non-muscle myosin IIB (1:200, #909901, BioLegend), and rat anti-BrdU (1:200, ab6326, Abcam). After 6x1-2h PBST washes, specimens were incubated 4°C overnight with AlexaFluor-conjugated secondaries (Life Technology). Nuclei and F-actin were counterstained respectively with DAPI (1:5000, 62247, Thermo Fisher Scientific) and AlexaFluor 488/635 Phalloidin (1:500, A12379, A34054, Invitrogen). Specimens were washed 6 times with PBST (1-2 hours per wash) then mounted on glass slides with 50% glycerol (#356352, Calbiochem) in PBS. Z-stacks were acquired by a confocal microscope (TCS SP5, Leica, Germany) using oil-immersion 40X and 63X objectives.

Morphometric analyses

Slice explants were imaged on a dissecting microscope with transmitted light brightfield optics. The contour of the basal side of the epithelium was manually traced in Fiji/ImageJ (Schindelin et al. 2012) and landmarks marked on the contours (Appendix **Fig. S1)**: Landmark coordinates were entered into the geometric morphometrics package MorphoJ (Klingenberg 2011) for Procrustes scaling (to separate size differences from shape differences) and statistically tested using the multiple permutation test (1000 permutations).

Cellular/nuclear analyses

Cellular/nuclear measurements used 40X z-stack images (0.21μm steps) of tooth germs from E13.5-E15.5 mT/mG mice. Only basal cells not undergoing mitosis (but including other cells with minimal basal contact) were measured. In E13.5, the corners in bottom one-third of the tooth bud were considered as cervical loops. Cells were measured in the optical slice containing their maximum cross-sectional area to avoid grazing artefacts. Morphological features were measured using Fiji tools. Nuclear position was defined as (distance between centroid and cell-base-midpoint)/ (cell height). Basal width was defined as a width of attachment to the basal membrane, and apical width was measured perpendicularly to the cell axis at 20% site from the cell apex (Appendix **Fig. S2**. Sample numbers are in Appendix Table S1.

Cell division orientation analysis

For cell division orientation, z-stack confocal images from mT/mG mice stained with DAPI were analysed. Only anaphase and telophase stages were selected. The acute angle relative to the basal lamina (90° = spindle perpendicular to the basal lamina) was measured in Fiji.

Statistics

All statistical analyses, except for cell division axis, were conducted with SPSS 24.0 (IBM). Comparison of tissue dimensions in the proliferation inhibition experiment was by Student's t-test. Comparison between multiple embryonic stages in cellular/nuclear measurements was analysed by ANOVA only (no post-hoc tests). For cell division orientation, Mardia-Watson-Wheeler tests (angle counterpart to the Mann-Whitney U-test, sensitive to both the mean and variance differences, although somewhat more to mean differences) were performed using R v3.5.0 (R Core Team 2013) and the package "circular" (Agostinelli et al. 2011). A value of $p < 0.05$ was considered statistically significant.

Results

Proliferation inhibition does not prevent bud-to-cap morphogenesis

To directly test the proposition that tooth bud-to-cap morphogenesis is caused by differential proliferation alone, we applied a proliferation inhibitor, aphidicolin to mouse molar tooth explants. Such explants faithfully recapitulate normal morphogenesis in culture (Alfaqeeh and Tucker 2013; Panousopoulou and Green 2016). Preliminary experiments showed that cultures with aphidicolin were healthy for one day but deteriorated after two days incubation (not shown). We therefore aphidicolin-treated explants and controls from E13.5, E14.0 and E14.5 embryos and imaged them after 3 and 23 hours to test for effects on morphogenesis, followed by a further 2h incubation with BrdU label to control for inhibition of proliferation. We confirmed inhibition of proliferation at the early time point, before significant morphogenesis had taken place (**Fig. 1B**), as well as at the final time-point. We found that at all stages tested, the treated explants were substantially smaller than controls showing growth arrest consistent with complete proliferation arrest (Appendix **Fig. S3**). Unexpectedly, despite the size difference, the epithelial shape changes were remarkably normal: non-proliferating tooth germs underwent the transition from smoothly rounded buds at E13.5 to more or less triangular shapes by E13.5+23h (**Fig. 2A,B**) and from the triangular shapes at E14.5 to a clear cap shape by E14.5 + 23h (**Fig.2E, F**). Shape change from E14.0 to E14.0 + 23h was less obvious (**Fig. 2C,D**). Qualitatively, the changes were very similar to those of the controls without inhibitor. To test this quantitatively, we used well-established geometric morphometrics (MorphoJ) (Klingenberg 2011) to compare the epithelial contours. We found no statistically significant difference ($p < 0.05$, multiple permutation T-squared test) between control and proliferation-inhibited shape. This strongly suggests that the models for bud-to-cap morphogenesis that depend exclusively on

differential proliferation do not reflect events in vivo. This finding raised the question as to what, if not proliferation, does drive the bud-to-cap transition?

Cell shape, nuclear position and spindle orientation analyses reveal basal expansion in cervical loops and basal contraction in inner dental epithelium

Most epithelial bending mechanisms involve cell shape changes from columnar to wedge-shaped (Pearl et al. 2017). To find out whether such cell shape changes occur in the tooth bud-to-cap transition, we quantified apical and basal dimensions, cell heights and nuclear positions in the different regions of the epithelium at the critical developmental stages. The results are shown in **Fig. 3**. Noting that some cells may shift between defined regions during development, we found that during this period, the apical-to-basal size ratio in the cervical loops (red line in Fig. 3C) declined steadily, concomitant with deepening invagination of the cervical loops. The ratio decreased partly due to apical reduction (Fig. 3B) but more due to basal expansion (Fig. 3A). The most dramatic change in apical-to-basal ratio, however, was in the inner dental epithelium (IDE) on either side of the enamel knot, which we call the "side IDE" at E14.5 (brown line in Fig. 3C). This corresponded to evagination of the side IDE relative to the bottom of the tooth bud to create the domed lining of the cap. The dramatic IDE ratio change was due to a sharp reduction of the basal size which outweighed a slight concomitant apical decrease. This reduction was so extreme that the bases of many of these cells were at the resolution of conventional confocal microscopy so the values plotted for their basal width and apical/basal ratio are maximum and minimum limits respectively. IDE cells' mitotic spindles seemed to be more vertically restricted compared to ODE spindles at E14.5 and E15.5 (**Fig. 3G**) perhaps because the cells also become highly columnarised although regulated orientation (to generate apical daughter cells, adding overlying stellate reticulum) could also be involved. Together the measurements shown in Fig. 3 reveal apical contraction and basal expansion in the cervical loops and basal contraction in the IDE during the bud-to-cap transition.

Actin/myosin localization indicates basal constriction in inner dental epithelium

To determine whether the observed cell shape changes were driven by active actomyosin mechanisms, we used fluorescent phalloidin to detect filamentous actin and immunofluorescence against myosin light chain followed by confocal imaging, noting that mechanical tension is well correlated with total myosin levels in other systems (Streichan et al. 2018 and Guy Blanchard, U. Cambridge, personal communication). At E13.5 myosin and actin were both relatively enriched in the suprabasal cells of the bud (**Fig. 4A-A"**), (consistent with its actively intercalating to make then narrow the bud neck (Panousopoulou and Green 2016)). Occasionally we saw slightly elevated myosin in regions at the base of prospective IDE cells at the bottom of the bud (**Fig. 4A',** arrowheads) although since apparent in only a few sections per specimen, this did not show up in averaged quantitations (**Fig. S4A,B**). At E14.0, there was a slight enrichment of myosin throughout the flattening bottom of the tooth germ (the prospective IDE and EK), smooth basally and punctate and

co-localized with actin apically (white foci in Fig. 4B). Some cells in the side-IDE showed even higher actin and myosin throughout (Fig. 4B', inset arrowheads). The outer dental epithelium was relatively depleted for myosin at this stage. Finally, at E14.5 there was myosin enrichment in the basally narrowing cells of the IDE, particularly basally, and concomitant depletion in the cervical loop and ODE (Fig. 4C-C" and Fig. S4). Taken together, these results show (1) basal actin and myosin enrichment coincident with basal contraction, indicating basal constriction in the IDE cells and (2) slight basal depletion and apical elevation of myosin in the outer cervical loops, suggesting some basal relaxation and apical constriction there.

Sensitivity of bud-to-cap transition to inhibition of Focal Adhesion Kinase (FAK) inhibition links it to other evaginations with basal constriction mechanisms

A well-studied example of basal contraction is the formation of the midbrain-hindbrain boundary constriction (Gutzman et al. 2008) which requires cell-matrix adhesion mediated by focal adhesion kinase (FAK) (Gutzman et al. 2018; Gutzman et al. 2008). To test whether the bud-to-cap transition involves similar mechanisms, we applied the FAK inhibitor PF-573228 to bud-stage explants. We found that, unlike aphidicolin, this clearly arrested epithelial morphogenesis: when controls had clearly progressed to the cap-stage morphology, the FAK inhibitor-treated explants remained bud-shaped (**Fig. 4D-G**). The treated explants were somewhat smaller, although not as small as the aphidicolin-treated explants (**Fig. S3B** versus **S3A**) but did incorporate BrdU (**Fig. 4G**), unlike the aphidicolin-treated explants, indicating at least some cell proliferation. Together these results showed that that even if proliferation and/or cell size may have been somewhat reduced by the FAK inhibitor, there was a clear effect on the bud-to-cap morphogenesis suggesting a common mechanism with basal constriction other contexts. As a side observation, we found that applying an inhibitor of Rho kinase, an activity that is involved very broadly in cell shape regulation, buds in explants became very enlarged and grossly deformed, rendering interpretation difficult.

Discussion

In this work we demonstrated in molar tooth slice explants that apparently normal epithelial shape change from bud to early cap is resistant to cell proliferation inhibition. This gross morphogenesis is therefore unlikely to be driven exclusively (and possibly at all) by differential cell proliferation, which has been proposed in previous models. Although there are caveats with explant experiments and use of inhibitors, the persistence of morphogenesis during well-controlled inhibition of proliferation is hard to explain away as an artefact of explantation or off-target inhibitor effects. Meanwhile, the proliferation inhibition was well controlled: initiated before any shape change, persisting to the end of the experiment, and resulting in complete growth arrest. Although a previously published proliferation-driven model (Marin-Riera et al. 2018) matched a detailed cell tracking dataset (Marin-Riera et al. 2018; Morita et al. 2016), the results reported here establish that the proliferation is likely

to be secondary to, rather than the cause of, the observed morphogenesis during the specific stages we tested.

We investigated alternative mechanisms that are based on cell shape change. Such changes were invisible to previous computational models because they treated the tissue either as a continuous material or as made of cells in the form of undeformable particles. Myosin was enriched where the cell domains got smaller and depleted where they expanded, indicating active, cell-autonomous mechanisms., especially during basal contraction in IDE adjacent to the enamel knot. In Drosophila, tension is quantitatively associated with total myosin (Streichan et al. 2018) and we consider this to be a good indicator of active constriction. Myosin phosphorylation is sometimes associated with activation but we found anti-phospho-myosin immunofluorescence somewhat unreliable. Importantly, we showed that inhibition of FAK is sufficient to arrest bud-to-cap morphogenesis, linking the latter to basal-constriction-dependent evagination at the midbrain-hindbrain border (Gutzman et al. 2018) and suggesting that further investigation of signals shown to be active in that system might also be acting in the tooth.

Can our results be reconciled with proliferation-based models and experiments? Mechanosensing can regulate proliferation so the latter could easily be downstream of the cell-autonomous shape changes we describe. Proliferation would thus facilitate normal morphogenesis even if not required for it. Additionally, while our proliferation-inhibited explants showed largely normal morphogenesis, subtle changes in the cell sizes and lineage distributions may have compensated for the lack of differential proliferation. Furthermore, we analysed a narrow stage range and it is possible that differential proliferation becomes increasingly important in later cap, bell and cusp formation.

We focused on epithelially autonomous mechanisms but experiments in which removal of the condensing mesenchyme caused the cervical loops to splay outwards at mid-to-late cap stages have shown clearly that physical constraint by the surrounding mesenchymal condensation is important for correct morphogenesis. This is perfectly compatible with our interpretations since those experiments were slightly later stages and mesenchyme removal reorientated the cervical loops but did not relax them or the epithelial bends adjacent to the enamel knot (Marin-Riera et al. 2018; Morita et al. 2016). A combination, summarised in **Fig. 5,** of autonomous proliferation-independent epithelial bending by basal constriction within an enclosing mesenchymal capsule thus provides a satisfying explanatory physical dual mechanism for molar morphogenesis from bud-to-bell stages.

The tooth germ is an outstanding model for developmental organogenesis and has played a major role in understanding gene action and epithelial-mesenchymal signaling. Its morphogenesis is no less interesting and our identification of basal relaxation and constriction in the cervical loops and IDE respectively is a first step towards integrating genetic and signalling aspects with the physical cell behaviours that make this organ.

Acknowledgements: This work was funded by BBSRC grant BB/P007325/1 to J.B.A.G. and a King's college London Dental Institute studentship to R.L. The authors have no conflicts of interest.

References

Agostinelli C, Lund U, Members P. 2011. Circular. 0.4-1 ed.

Alfaqeeh SA, Tucker AS. 2013. The slice culture method for following development of tooth germs in explant culture. J Vis Exp. (81):e50824.

Gutzman JH, Graeden E, Brachmann I, Yamazoe S, Chen JK, Sive H. 2018. Basal constriction during midbrain-hindbrain boundary morphogenesis is mediated by wnt5b and focal adhesion kinase. Biol Open. 7(11).

Gutzman JH, Graeden EG, Lowery LA, Holley HS, Sive H. 2008. Formation of the zebrafish midbrain-hindbrain boundary constriction requires laminin-dependent basal constriction. Mech Dev. 125(11-12):974-983.

Jernvall J, Kettunen P, Karavanova I, Martin LB, Thesleff I. 1994. Evidence for the role of the enamel knot as a control center in mammalian tooth cusp formation: Non-dividing cells express growth stimulating fgf-4 gene. The International journal of developmental biology. 38(3):463-469.

Kieffer S, Peterkova R, Vonesch JL, Ruch JV, Peterka M, Lesot H. 1999. Morphogenesis of the lower incisor in the mouse from the bud to early bell stage. The International journal of developmental biology. 43(6):531-539.

Klingenberg CP. 2011. Morphoj: An integrated software package for geometric morphometrics. Mol Ecol Resour. 11(2):353-357.

Li J, Chatzeli L, Panousopoulou E, Tucker AS, Green JB. 2016. Epithelial stratification and placode invagination are separable functions in early morphogenesis of the molar tooth. Development. 143(4):670-681.

Marin-Riera M, Moustakas-Verho J, Savriama Y, Jernvall J, Salazar-Ciudad I. 2018. Differential tissue growth and cell adhesion alone drive early tooth morphogenesis: An ex vivo and in silico study. PLoS Comput Biol. 14(2):e1005981.

Mikkola ML, Millar SE. 2006. The mammary bud as a skin appendage: Unique and shared aspects of development. J Mammary Gland Biol Neoplasia. 11(3-4):187-203.

Morita R, Kihira M, Nakatsu Y, Nomoto Y, Ogawa M, Ohashi K, Mizuno K, Tachikawa T, Ishimoto Y, Morishita Y et al. 2016. Coordination of cellular dynamics contributes to tooth epithelium deformations. PLoS ONE. 11(9):e0161336.

Panousopoulou E, Green JB. 2016. Invagination of ectodermal placodes is driven by cell intercalation-mediated contraction of the suprabasal tissue canopy. PLoS Biol. 14(3):e1002405.

Pearl EJ, Li J, Green JB. 2017. Cellular systems for epithelial invagination. Philosophical transactions of the Royal Society of London. 372(1720).

Peterkova R, Lesot H, Vonesch JL, Peterka M, Ruch JV. 1996. Mouse molar morphogenesis revisited by three dimensional reconstruction. I. Analysis of initial stages of the first upper molar development revealed two transient buds. The International journal of developmental biology. 40(5):1009-1016.

Pispa J, Thesleff I. 2003. Mechanisms of ectodermal organogenesis. Developmental biology. 262(2):195-205.

R Core Team. 2013. R: A language and environment for statistical computing. Vienna, Austria: R Foundation for Statistical Computing.

Salazar-Ciudad I, Jernvall J. 2002. A gene network model accounting for development and evolution of mammalian teeth. Proceedings of the National Academy of Sciences of the United States of America. 99(12):8116-8120.

Salazar-Ciudad I, Jernvall J. 2010. A computational model of teeth and the developmental origins of morphological variation. Nature. 464(7288):583-586.

Schindelin J, Arganda-Carreras I, Frise E, Kaynig V, Longair M, Pietzsch T, Preibisch S, Rueden C, Saalfeld S, Schmid B et al. 2012. Fiji: An open-source platform for biological-image analysis. Nat Methods. 9(7):676-682.

Shyer AE, Tallinen T, Nerurkar NL, Wei Z, Gil ES, Kaplan DL, Tabin CJ, Mahadevan L. 2013. Villification: How the gut gets its villi. Science (New York, NY. 342(6155):212-218.

Streichan SJ, Lefebvre MF, Noll N, Wieschaus EF, Shraiman BI. 2018. Global morphogenetic flow is accurately predicted by the spatial distribution of myosin motors. Elife. 7.

Takigawa-Imamura H, Morita R, Iwaki T, Tsuji T, Yoshikawa K. 2015. Tooth germ invagination from cell-cell interaction: Working hypothesis on mechanical instability. Journal of theoretical biology. 382:284-291.

Ten Cate AR, Sharpe PT, Roy S, Nanci A. 2012. Development of the tooth and its supporting tissues. In: Nanci A, editor. Ten cate's oral histology: Development, structure, and function. St. Louis:: Elsevier Mosby. p. 70-94.

Thesleff I. 2003. Epithelial-mesenchymal signalling regulating tooth morphogenesis. Journal of cell science. 116(Pt 9):1647-1648.

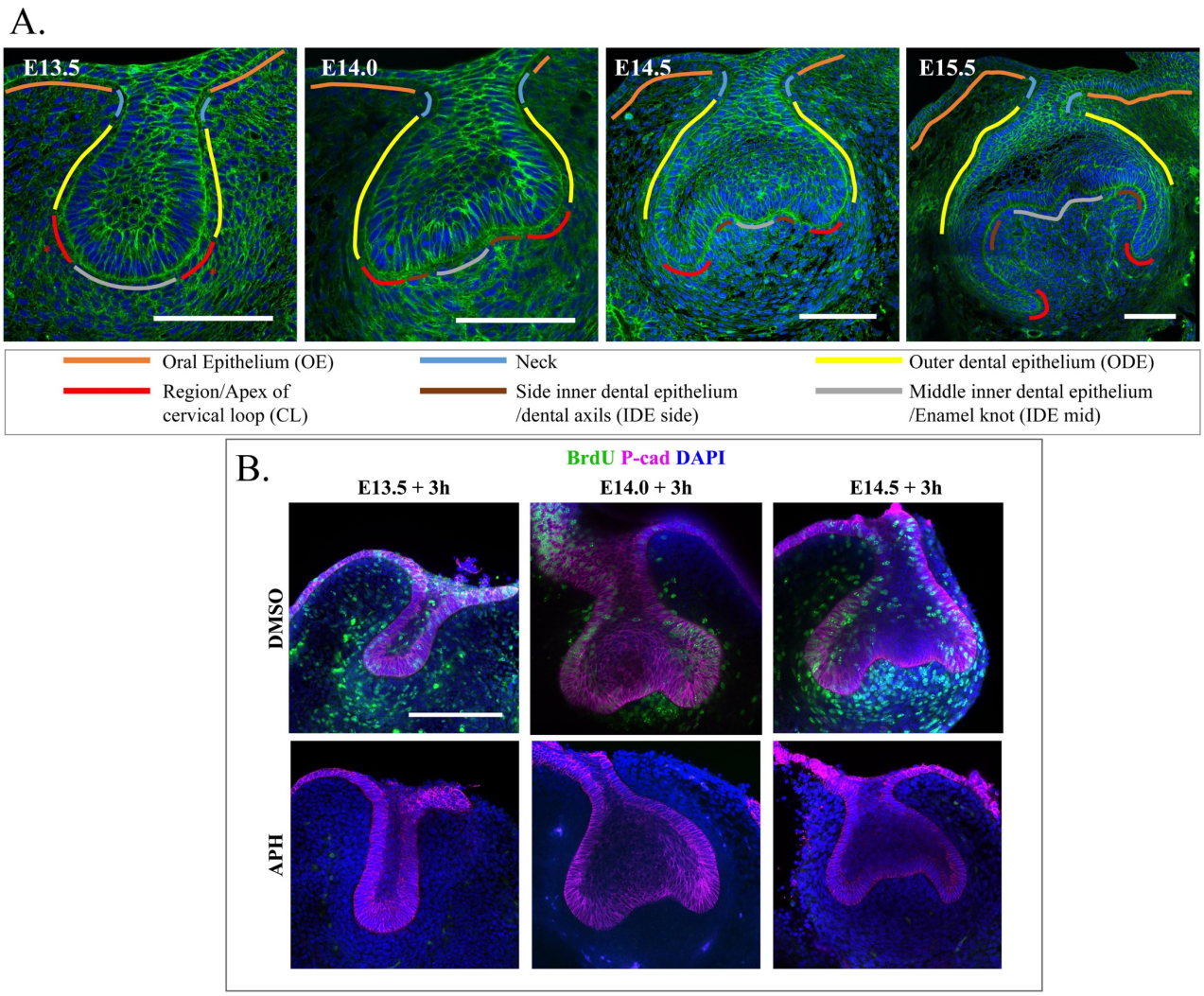

Fig.1 Molar tooth germs show dynamic shape change from bud to cap to bell stages

A. Confocal images of frontally sliced tooth germs at the indicated stages stained with phalloidin (green) for f-actin and DAPI (blue) for nuclei. Scale bar = 100μm. B. Confocal images of tooth germ explants made at the stages shown treated with aphidicolin (APH) or vehicle as indicated, incubated for 3 hours and labelled for a further 2 hours with BrdU (green). Counterstains are DAPI (nuclei, blue) and P-cadherin (magenta). Absence of green label with aphidicolin treatment shows complete inhibition of proliferation while cells in the control group actively proliferated at 3 hours of treatment. Scale bar = 100μm for all panels.

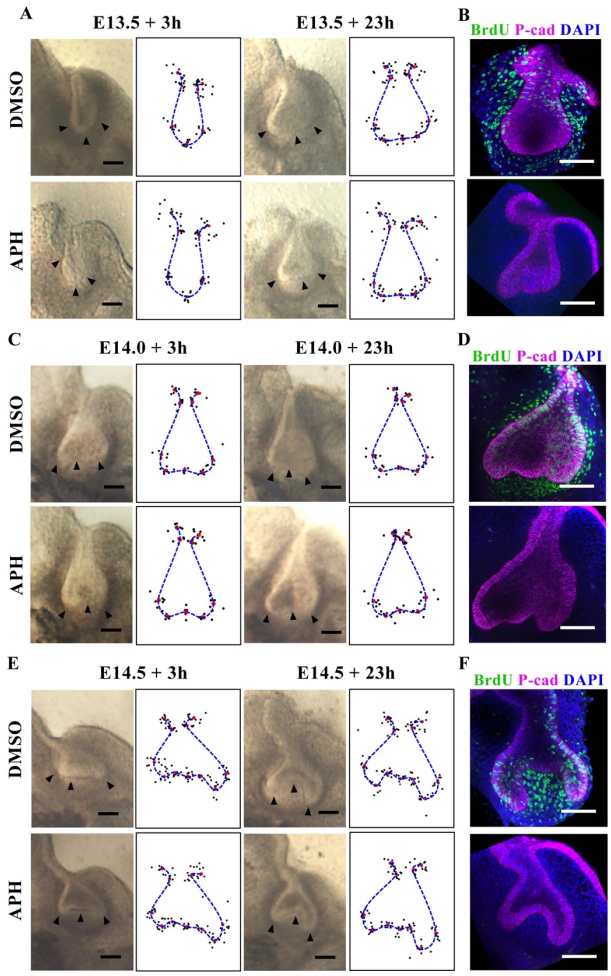

Fig. 2 Proliferation inhibition does not inhibit tooth explant bud-to-cap morphogenesis

(A, C, E) Typical brightfield images of tooth explants with or without aphidicolin (APH) at the times indicated together with corresponding epithelial landmark- and contour-plots for multiple samples (n = 10 explants from three different litters for E13.5 and 14.5, n = 6 explants from one litter for E14.0). Small black dots show positions of individual landmarks, red dots show average position of each landmark and blue dashed line indicates average contour. (B, D, F) Confocal images of explants shown in A, C, and E, labelled for a further 2 hours with BrdU (green) confirming that proliferation is inhibited by aphidicolin. Scale bar=100μm.

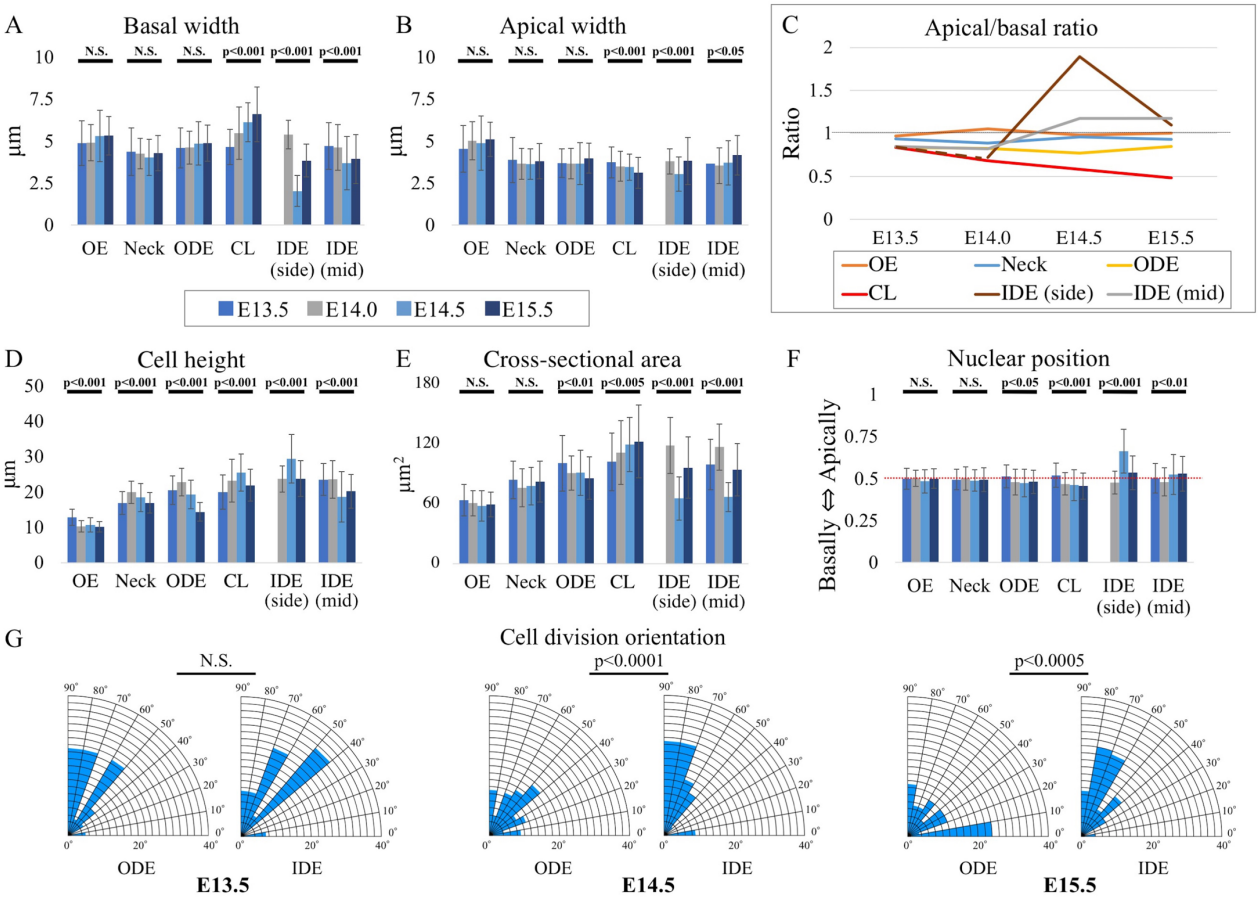

Fig.3 The cellular/nuclear shape analysis of epithelial cells of tooth germs show basal expansion in the cervical loops and basal contraction in the inner dental epithelium during bud-to-cap transition

Measurements from middle optical sections of membrane-labelled cells. (A-C) Cervical loop (CL) cells showed a significant increase in basal width and a slight decrease in apical width (columnar to wedge-shape change) from E13.5 to E15.5 while IDE (side) cells were significantly contracted basally at E14.5. (D,E) Cell heights and areas showing mostly increases but area decrease in IDE at E14.5. (F) Apicobasal position of nuclei in basal cells showing central position except for at IDE (side) where nuclei were more apical at E14.5. (G) Spindle-to-lamina angles were all vertical-to-oblique (i.e. 45°-90°) at E13.5 but were more randomly orientated in the ODE at E14.5 and E15.5. n = 60 cells/region/stage for A-F, n = 38-87 in G. (See Appendix Table S1 for sample number details),

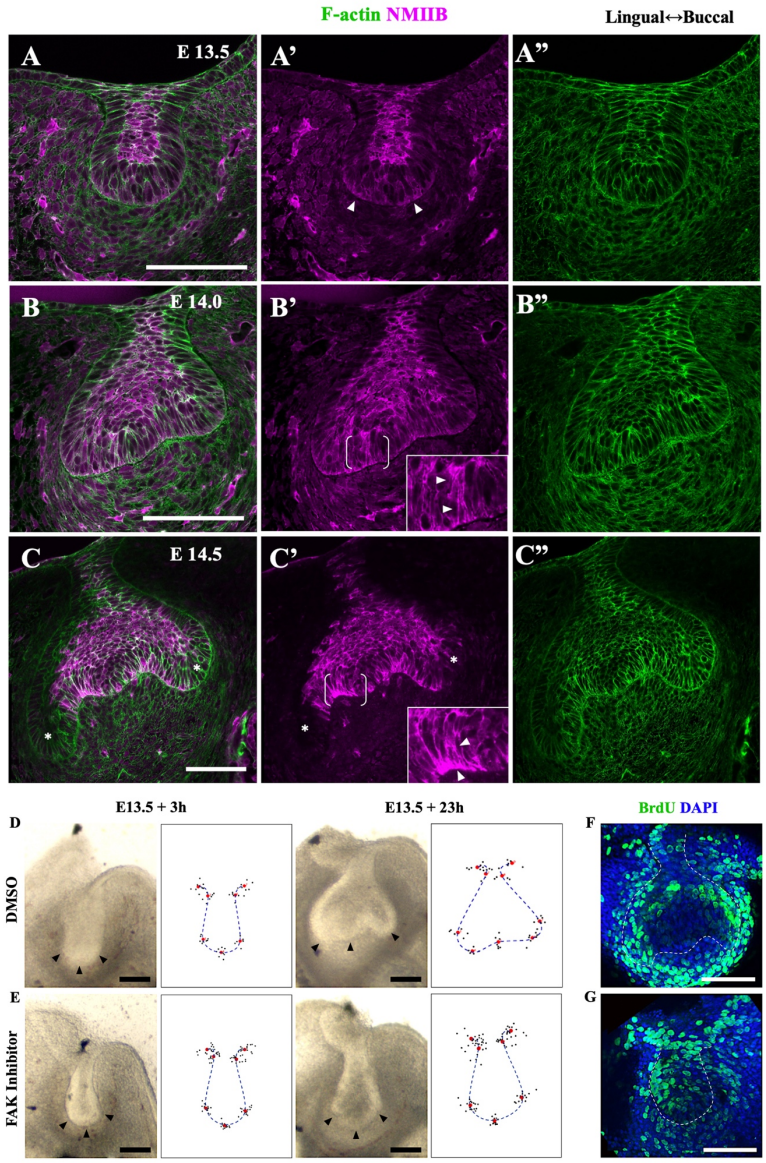

Fig. 4 Confocal images of Myosin Ⅱ B and F-actin in tooth germs show markers of basal relaxation in the cervical loops and basal constriction in the inner dental epithelium during bud-to-cap transition

Confocal images of fixed mandible slices stained for f-actin (green) and non-muscle myosin IIA (NMIIB) (magenta) at E13.5 (A-A"), E14.0 (B-B") and E14.5 (C-C"). At 13.5 NMIIB is accumulated throughout the suprabasal cells of the bud and sometimes weakly either side of the base of the bud (arrowheads in A'). (B) At 14.0 NM Ⅱ B localises in the suprabasal cells as well as the basal surface of the flattened bottoms of tooth germ and more highly throughout some IDE cells (arrowheads in inset close-up of bracketed region). Strong co-accumulation of NMIIB and F-actin is sparsely found at apical sites of basal cells particularly around prospective cervical loops and the circumferential regions of enamel knot. (C) At E14.5 there is an obvious enrichment of NMIIB and F-actin at the basal sides of IDE, which corresponds to the peripherical enamel knot where basally-narrowing cells are aligned (arrowheads in inset close-up of bracketed region).

(D, E) Typical brightfield images of tooth explants with or without FAK inhibitor at the times indicated together with corresponding epithelial landmark- and contour-plots for multiple samples (n = 16 and 8 for inhibitor-treated and controls respectively from three different litters. Small black dots show positions of individual landmarks, red dots show average position of each landmark and blue dashed line indicates average contour. (F, G) Typical confocal images of explants labelled for a further 2 hours with BrdU (green) showing that proliferation persists in FAK inhibitor-treated explants.

Scale bars = 100μm.

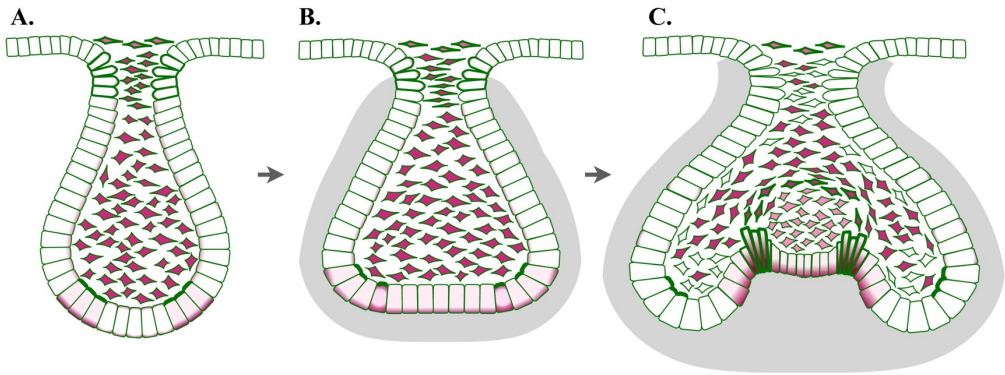

Fig. 5 Schematic summarising cell shape and cytoskeletal changes during bud-to-cap transition.

A. Bud-stage molar has elevated actin (green) in the elongated cells of the neck (associated with prior cell intercalation) and high myosin (maroon) in all suprabasal cells. Localised elevation of basal myosin, moderately in most of the cell (pink) and high at the basal end (maroon) in cells at the bottom of the bud on either side of the midline pre-figures basal constriction of some cells. **B.** Cells at the base of the bud have elevated myosin as this prospective inner dental epithelium flattens. The mesenchyme (grey) begins to condense around the epithelium. **C.** Actin and myosin are sharply elevated in cells of the inner dental epithelium which radically change their shape, becoming highly columnar and narrowing basally through basal constriction to evaginate the epithelium on either side of the central enamel knot. This creates the cap shape while surrounding mesenchyme constrains the cervical loops to point downwards.

Appendix: Supplementary Figures & Table

Appendix Fig. S1 Landmarks and dimensional measures used for quantifications in Fig. S3

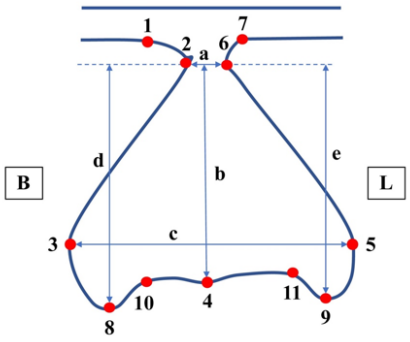

Landmarks
1: Limit of flatter epithelium (B = buccal)
2: Narrowest point at neck (B)
3: Buccal-most point in germ body
4: Mid-Bottom
5: Lingual-most point in germ body
6: Narrowest point at neck (L = lingual)
7: Limit of flatter epithelium (L)
8: Bottom of cervical loop (B) *
9: Bottom of cervical loop (L) *
10: Transitional point from inner dental epithelium to cervical loop (B) **
11: Transitional point from inner dental epithelium to cervical loop (L) **

Tooth germ size: taken as area enclosed by basal lamina contour and straight line between landmarks 1 and 7

Measured width/length
a: Neck width
b: Germ height
c: Germ body width
(d-b): Length of cervical loop (B) **
(e-b): Length of cervical loop (L) **

* ED 14.0 and ED 14.5 only
** ED 14.5 only

Appendix Fig. S2 Cell Shape measurements

Upper panels show example confocal sections of molar regions indicated from mTmG embryos with membranes labelled by membrane-Tomato fluorescent protein (magenta) and nuclei stained with DAPI (blue). Lower panels show cell outlines with example measurements of basal attachment (b-b'), cell apex (a) and apical width (aw-aw') at 20% below the apex along the cell axis (line from apex to midpoint of base). Note that every cell to be measured was inspected at multiple z-sections to resolve any ambiguities (e.g. checking that only cells that made contact with the basal lamina were considered) and measured at its largest section to avoid grazing artefacts.